Supplement of

Measurement report: High contribution of N_2O_5 uptake to particulate nitrate formation in NO_2-limited urban areas

Ziyi Lin[1,2,3], Chuanyou Ying[4], Lingling Xu[1,2*], Xiaoting Ji[1,2,3], Keran Zhang[1,2], Feng Zhang[2], Gaojie Chen[1,2,3], Lingjun Li[1,2,3], Chen Yang[1,2,3], Yuping Chen[1,2,3], Ziying Chen[1,2,3], Jinsheng Chen[1,2*]

Affiliations:

[1]State Key Laboratory of Advanced Environmental Technology, Institute of Urban Environment, Chinese Academy of Sciences, Xiamen 361021, China

[2]Fujian Key Laboratory of Atmospheric Ozone Pollution Prevention, Institute of Urban Environment, Chinese Academy of Sciences, Xiamen 361021, China

[3]University of Chinese Academy of Sciences, Beijing 100049, China

[4]Fuzhou Institute of Environmental Science, Fuzhou 350013, China

**Correspondence to*: Jinsheng Chen (jschen@iue.ac.cn); Lingling Xu (linglingxu@iue.ac.cn)

TABLE OF CONTENTS

Supplementary Texts

S1. Measurements techniques.

The O_3, NO*x*, $PM_{2.5}$, SO_2, and CO were monitored by Thermo Instrument 49*i*, 17*i*, 1405DF, 43*i*, and 48*i* (Thermo Fisher Scientific, Waltham, MA, USA), respectively. Water-soluble gas (HONO) and water-soluble inorganic ions (sulfate, nitrate, ammonium and chloride) were measured by an online analyzer (MARGA ADI 2080, Applikon Analytical B.V, Netherlands). Organic carbon and elemental carbon in $PM_{2.5}$ were measured by OC/EC analyzer (Model 4, Sailhero Environmental Protection High-tech Co., Heibei, China). Around 106 species of VOCs were observed in hourly interval by a gas chromatography-mass spectrometer (GC-FID/MS, TH-300B, Wuhan, CN). As for HCHO and PAN, they were measured by the HCHO analyzer (FMS-100, Focused Photonics Inc., Hangzhou, China) and the PAN analyzer (PANs-1000, Focused Photonics Inc., Hangzhou, China), respectively. In addition, ambient temperature (T), relative humidity (RH), atmospheric pressure (P), wind speed (WS), and wind direction (WD) were measured by an integrated sensor (150WX, Airmar, Milford, NH, USA). The photolysis frequencies (JO_1D, JNO_2, JHONO, JNO_3, JHCHO and JH_2O_2) were measured by a photolysis spectrometer (FPS-100, Focused Photonics Inc., Hangzhou, China). The uncertainty and detection limit of above observing instruments were described in our previous studies (Liu et al., 2022a; Liu et al., 2023; Hu et al., 2022; Hu et al., 2020; Liu et al., 2022b; Yang et al., 2023).

S2. Detailed settings of Iodide-TOF-CIMS and the calibrations of N_2O_5 and $ClNO_2$.

In this work, the chemical ionization atmospheric pressure interface long-time-of flight mass spectrometer (API-ToF-CIMS, Aerodyne Research Inc., USA) with an iodide source was used to detect ambient N_2O_5 and $ClNO_2$. A stainless-steel tube with a length of near 2 meters and a diameter of 1/4 inch inner diameter was used for sampling. The sampling flow rate was set as 10 standard liters per minute (SLPM) and only 2SLPM from the total flow was diverted to the CIMS. The nitrogen (N_2) flow (99.999%, 2.7 SLPM) containing the methyl iodide gas (CH_3I) released by a heated CH_3I permeation tube cylinder, passed through a soft X-ray device (Tofwerk AG, P-type) to generate reagent ions I^-. The I- was combined with the target gas in ion molecule reaction (IMR) chamber and then detected by ToF-CIMS instrument. The ambient N_2O_5 and $ClNO_2$ were detected as $I(N_2O_5)^-$ and $I(ClNO_2)^-$ clusters at 235 and 238 m/z. In order to minimize the effect of particles deposited on the surface of the sampling inlet, the tube was cleaned by deionized water and dried by nitrogen flow once a week.

The calibration of N_2O_5 and $ClNO_2$ was set similar to previous studies (Wang et al., 2022b; Wang et al., 2022a; Thaler et al., 2011). And the calibration of N_2O_5 is based on the already calibrated $ClNO_2$. Briefly, during the $ClNO_2$ calibration process, a N_2 flow (50 mL min^{-1}) containing 6 ppmv Cl_2 was passed over a slurry containing $NaNO_2$ and NaCl to produce $ClNO_2$ and then the mixed flow was sampled into the CIMS instrument under a certain RH. The function of NaCl was minimizing formation of NO_2 as a byproduct. To quantify $ClNO_2$, the mixed flow was fed directly into a cavity attenuated phase shift spectroscopy instrument (CAPS) or passed through a thermal dissociation tube at 380 ℃ before being fed into the CAPS to measure the background NO_2 and the total NO_2 (background NO_2 and the NO_2 decomposed by $ClNO_2$), respectively. The difference between the total NO_2 and background NO_2 was equivalent to the concentration of $ClNO_2$. And the normalized signal of $ClNO_2$ was tested in different RH conditions. To calibrate the N_2O_5, the stable flow of N_2O_5 was produced by mixing the O_3 flow and NO_2 flow. The O_3 oxidized NO_2 to from NO_3, which was further oxidized to from N_2O_5. Under different certain RH, the stable-N_2O_5 flow was sampled into CIMS instrument to obtain a normalized signal for N_2O_5 varying with RH. Subsequently, we delivered the N_2O_5 flow at ~50% RH through a supersaturated sodium chloride solution to convert N_2O_5 to $ClNO_2$ and then sampled in to CIMS. The concentration of N_2O_5 was delivered at ~ 50% RH by already calibrated $ClNO_2$ and then scaled to other RH conditions by the normalized N_2O_5 signal, which was mentioned above. The final calibration files for N_2O_5 and $ClNO_2$ at different RH are shown as **Figure S2**. The detection limit of N_2O_5 and $ClNO_2$ were 1.3 and 0.43 ppt, respectively.

S3. The interactive box model.

The interactive box model considers five main chemical reactions related to N_2O_5 (see **R1 – R5**). Reaction rate of k_1 and reversible reaction k_{eq} are $1.2\times10^{-13}\ e^{-2450/T}$ and $2.7\times10^{-27}\ e^{11000/T}$, respectively.(Demore et al., 1997; Brown et al., 2003b) Measured O_3, NO_2, N_2O_5, $ClNO_2$, VOCs and meteorological parameters during the observation period were used to constrain the model simulation. The hourly NO_3 reactivity with VOCs was estimated from the sum of measured VOCs concentrations and reaction rate coefficients of MCM v3.3.1 (Atkinson and Arey, 2003; Wang et al., 2017; Jenkin et al., 2003; Jenkin et al., 2015). Due to the lack of measurements for biogenic monoterpenes, the calculated NO_3 reactivity could be considered as a lower limit. Procedure of this model, as presented in other studies (Chen et al., 2020; Niu et al., 2022), includes a backward integration step to get simulated concentration

of O_3 and NO_2, a forward integration step to get simulated concentration of NO_3 and N_2O_5, a calculating the first-order loss rate of N_2O_5 (kN_2O_5) step and an adjusting step to reduce the difference between simulated and measured N_2O_5 to less than 1%. The $ClNO_2$ production rate ($\varphi ClNO_2$) was calculated by **eq 1**. The initial time for each model simulation was set to the sunset time, with a total duration of 24 hours.

$$O_3+NO_2 \xrightarrow{k1} NO_3+O_2 \quad (R1)$$

$$NO_2+ NO_3 \xrightarrow{k2f} N_2O_5 \quad (R2)$$

$$N_2O_5 \xrightarrow{k2r} NO_2+ NO_3 \quad (R3)$$

$$NO_3+VOCs \xrightarrow{kNO_3} products \quad (R4)$$

$$N_2O_5+H_2O/Cl^-(p) \xrightarrow{kN_2O_5} pNO_3(particle)+ClNO_2 \quad (R5)$$

S4. The steady-state method.

The input data was also from the 2022 winter observation. Based on the basic framework of the nighttime N_2O_5 chemistry described in **R1 – R5** and 5-minute resolution data of N_2O_5, NO_2, O_3, and T, the lifetime of N_2O_5 (τN_2O_5) is estimated by the **eq 3** with K_{eq} (calculated by the **eq 2**) in assumption of the steady state (Brown et al., 2003a). The robust kN_2O_5 could be derived by the **eq 4** as an intercept (Chen et al., 2022).Similarly, the ($\varphi ClNO_2$) was calculated by the **eq 1**. Notably, the results are summarized in **Table S6.**

$$\varphi ClNO_2=\frac{[ClNO_2]}{\int kN_2O_5\,[N_2O_5]dt} \quad (1)$$

$$K_{eq}(T)=2.7\times10^{-27}e^{11000/T} \quad (2)$$

$$\tau_{N_2O_5}=\frac{[N_2O_5]}{K_1(T)[NO_2][O_3]} \quad (3)$$

$$(\tau_{N_2O_5})^{-1}=kN_2O_5+\frac{k_{NO_3}}{K_{eq}[NO_2]} \quad (4)$$

S5. Setting of the multiphase chemical box model

The F0AM model was used to simulated the formation rate of pNO_3^- by different formation pathways. Measured hourly interval data of trace gases (VOC_s, O_3, NO, NO_2, CO, SO_2), photochemically active species (HONO, HCHO, PAN), meteorological variables (temperature, relative humidity,

atmospheric pressure, and photolysis frequencies), reanalysis data (boundary layer height, surface albedo and overhead ozone column) and simulated heterogeneous parameters in wintertime of 2022 as summarized in **Table S5** were used to constrain this model. It should be noted that the photolysis rate constants of the model parameterization were corrected by the observed and simulated photolysis rates of NO_2, except observed photolysis frequencies. To better simulate the concentration of intermediate species, 3-day spin-up was set before each model simulation. In addition to chemical processes, physical loss processes including dry deposition and dilution were also considered in this model including dry deposition and dilution process. The dry deposition velocity for the constrained species was set as Liu et al (Liu et al., 2022b). The basic dilution rate was 2×10^{-5} s^{-1} and varied with the boundary height. The incorporated mechanisms in the F0AM model are presented as **Table S2**.

S6. Detailed information about explainable machine learning techniques

(1) Setting of XGBoost model and validation.

Extreme gradient boosting (XGBoost) model was used to explore the influencing factors of N_2O_5 uptake. The input data for the model were hourly data at night (18:00 – 06:00 the next day) during winter 2022. The dataset including 813 samples was divided into a training set (80%) and a test set (20%). The hyperparameters were tuned using grid search and cross-validation methods. Specifically, for a single hyperparameter, grid search was used to obtain its more appropriate value range. For combinations of hyperparameters, the whole training set was split into ten folds. Grid search was then conducted over the pre-adjusted combinations of hyperparameters by training on nine folds and predicting on the tenth fold, following a cross-validation procedure. The hyperparameters of the final model were determined according to the R^2 function score. For the key hyperparameters of the XGBoost model in this study, the number of trees was 100, the learning rate was 0.07, the max depth was 7 and the regularization parameter lambda was set as 1.38.

The established model was evaluated by three statistical indicators including R^2 value, Mean Absolute Error (MAE) and Root Mean Square Error (RMSE). The R^2 is used to judge the goodness of fit between the predicted and observed results. The MAE provides a measure of predicted and observed results. And the RMSE characterizes the predictive accuracy of the model. The equations to calculate R^2, MAE and RMSE are **eq 5**, **eq 6**, and **eq 7**, respectively. The XGBoost model built in this study performed well, with an R^2 of 0.97, an MAE of 0.07, and an RMSE of 0.14 (**Figure S5**).

$$R^2=1-\frac{\sum_{i=1}^{N}(y_i - y'_i)^2}{\sum_{i=1}^{N}(y_i - \overline{y})^2} \quad (5)$$

$$MAE=\sqrt{\frac{\sum_{i=1}^{N}(y_i - y'_i)^2}{N}} \quad (6)$$

$$RMSE=\frac{1}{N}\sum_{i=1}^{N}|y_i - y'_i|^2 \quad (7)$$

Where y_i, y'_i, $\overline{y}$, and N refer to the actual value of the *i*-th sample, the simulated value of the *i*-th sample, the mean of the actual values of all samples, and N is the number of samples, respectively.

(2) The Shapley Additive Explanation theory

In this study, the target of SHAP method is to find the drivers of N_2O_5 uptake. The SHAP method could quantified the contribution of each feature to the variation of N_2O_5 uptake. Based on the coalitional game theory (Shapley, 1953), SHAP values were computed according to **eq 8** and describe the contribution of each feature to the prediction of an individual sample relative to the base prediction value of all samples.

$$g(x_i)=\phi(x)_{base}+\sum_{j=1}^{M}\phi(x_{i,j}) \quad (8)$$

Where $g(x_i)$ is a predicted value for each sample x_i containing M features, $\phi(x)_{base}$, the base value, represents the predicted value for all samples. $\phi(x_{i,j})$ is the SHAP value of the feature j in sample x_i showing its impact on the prediction. In this study, the importance of input variables to variation of N_2O_5 uptake was quantified by absolute SHAP values. SHAP > 0 means that the feature has a positive impact to N_2O_5 uptake relative to the base value. While conversely, it exerts a negative contribution.

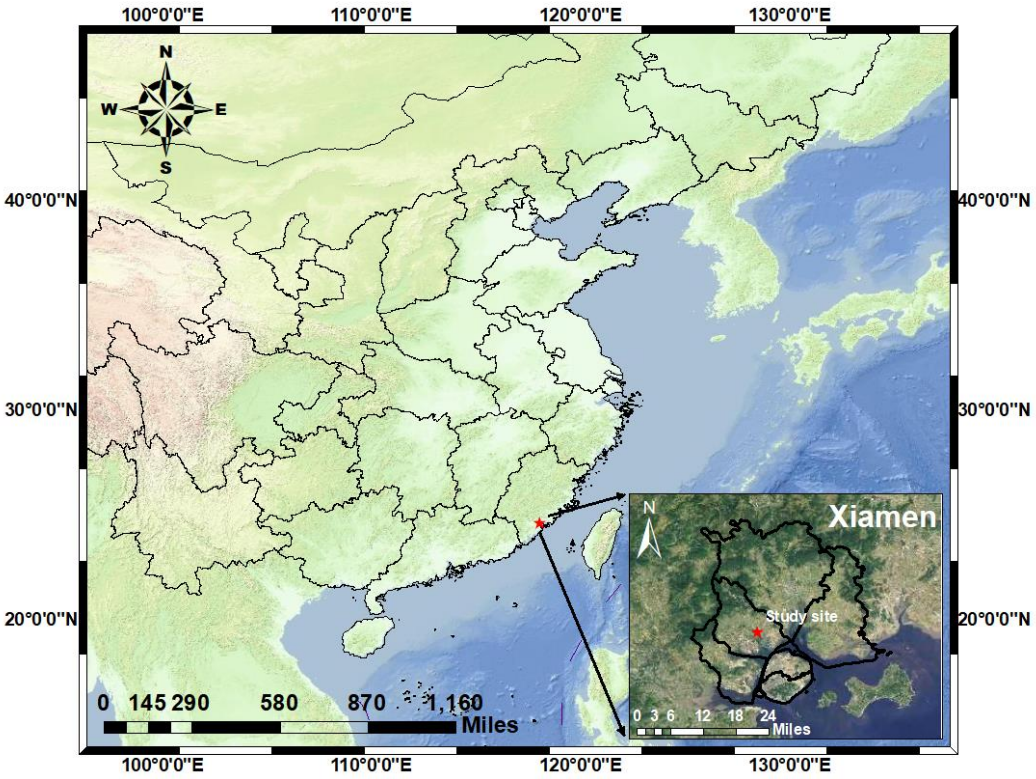

171

172 **Figure S1.** Measurement site located in the Atmospheric Observation Supersite of Institute of Urban
173 Environment, Chinese Academy of Science (red star; 24.61°N, 118.06°E) in Xiamen city of Southeast
174 China. The observation site is approximately 70 meters above ground level and surrounded by the
175 educational institutions, residential buildings, and traffic arteries, thereby, representing a typical urban
176 site.

177

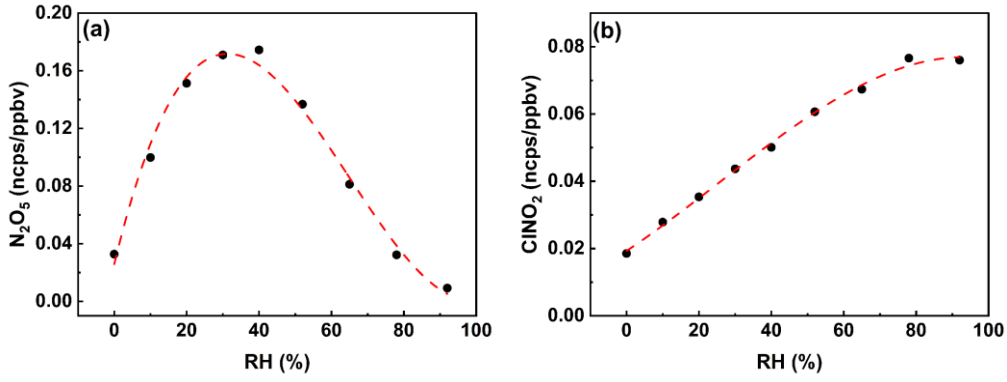

178

179 **Figure S2.** The calibration curve of CIMS instrument as a function of relative humidity (RH) for **(a)**
180 N_2O_5 and **(b)** $ClNO_2$.

181

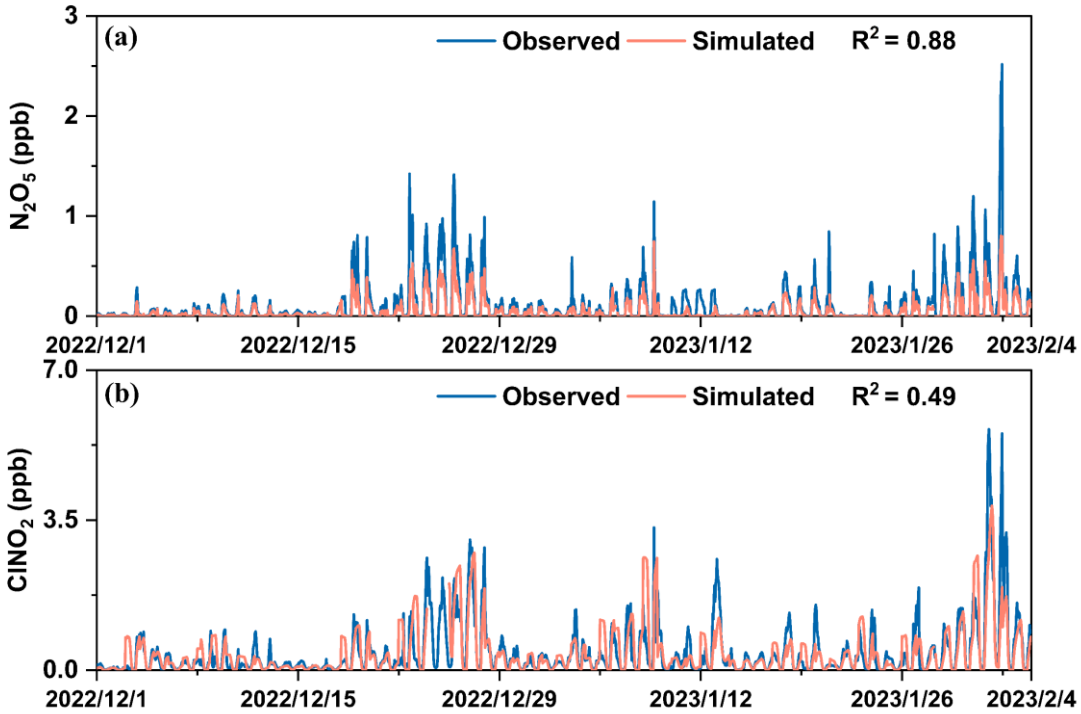

182

183 **Figure S3.** Time series of the observed and simulated **(a)** N_2O_5 and **(b)** $ClNO_2$ from the multiphase

184 chemical box model, respectively.

185

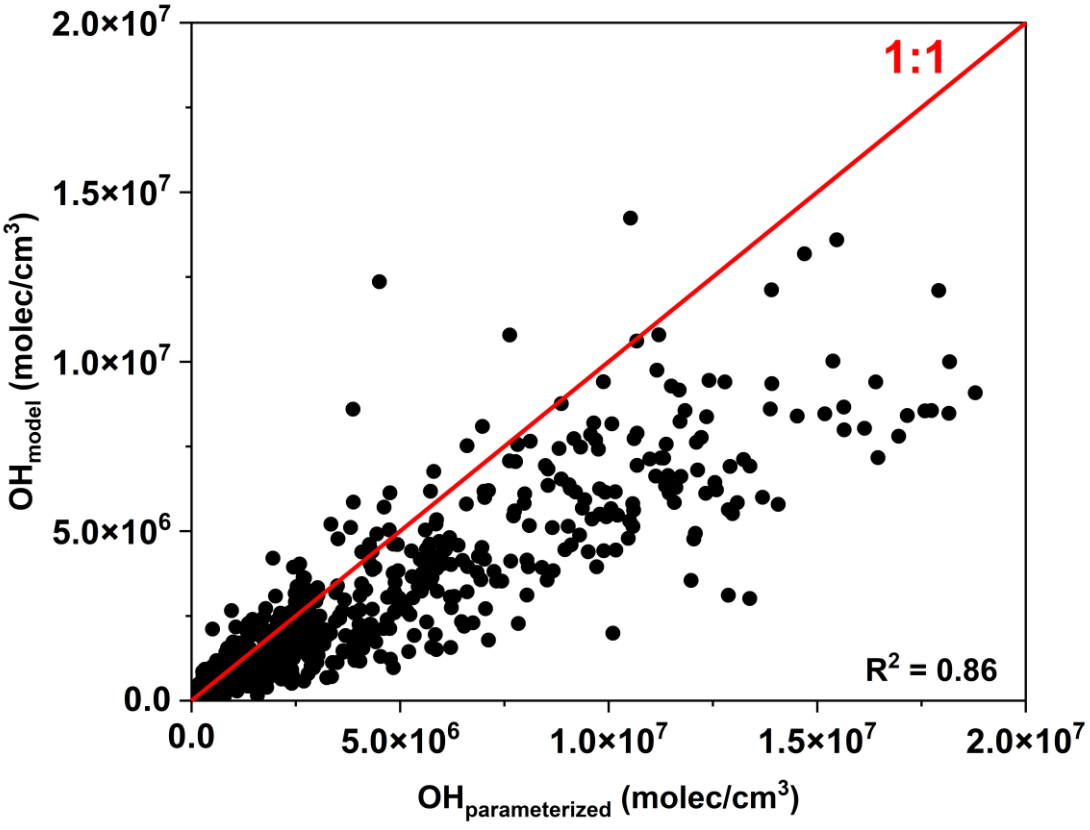

186

187 **Figure. S4.** Concentration of OH radical derived from parameterized method and F0AM model

simulation. The method of OH parameterization was suggested by Ehhalt and Rohrer (Ehhalt and Rohrer, 2000): $[OH]=4.1\times10^{9}\times(J_{O1D})^{0.83}\times(J_{NO2})^{0.19}\times\frac{140\times[NO_2]+1}{0.41\times[NO_2]^2+1.7\times[NO_2]+1}$

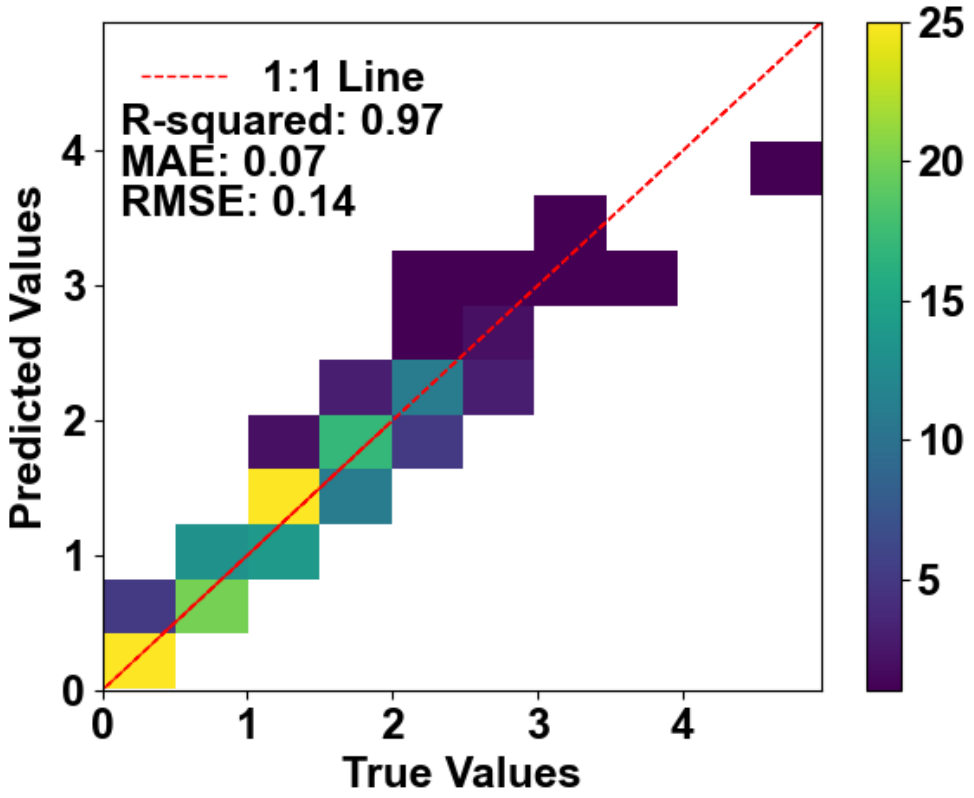

Figure S5. Performance of the XGBoost model based on the test set. The color bar is colored with number density.

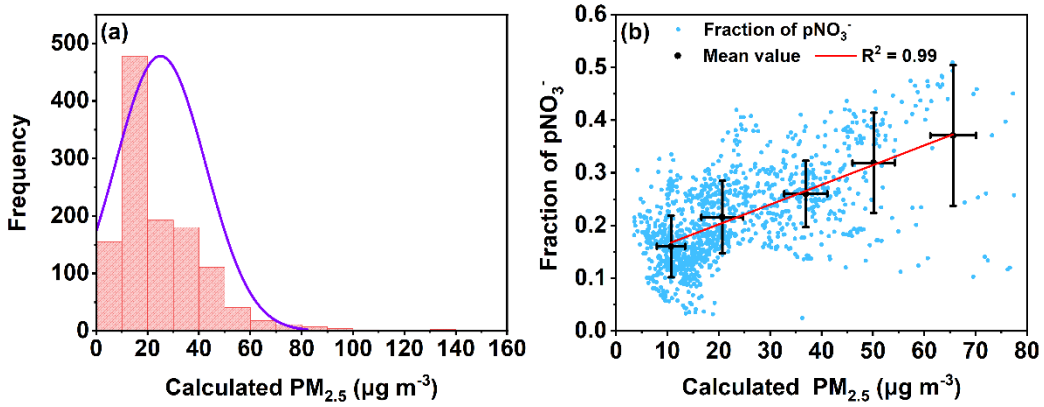

Figure S6. Histogram of the distribution of hourly calculated $PM_{2.5}$ concentrations **(a)** and variation of nitrate fractions with the levels of the hourly calculated $PM_{2.5}$ concentrations **(b).** The calculated $PM_{2.5}$ concentration is the summed concentration of major chemical components, including water-soluble

199 inorganic ions, trace elements, organic carbon and elemental carbon. Error bar represents one standard

200 deviation.

201

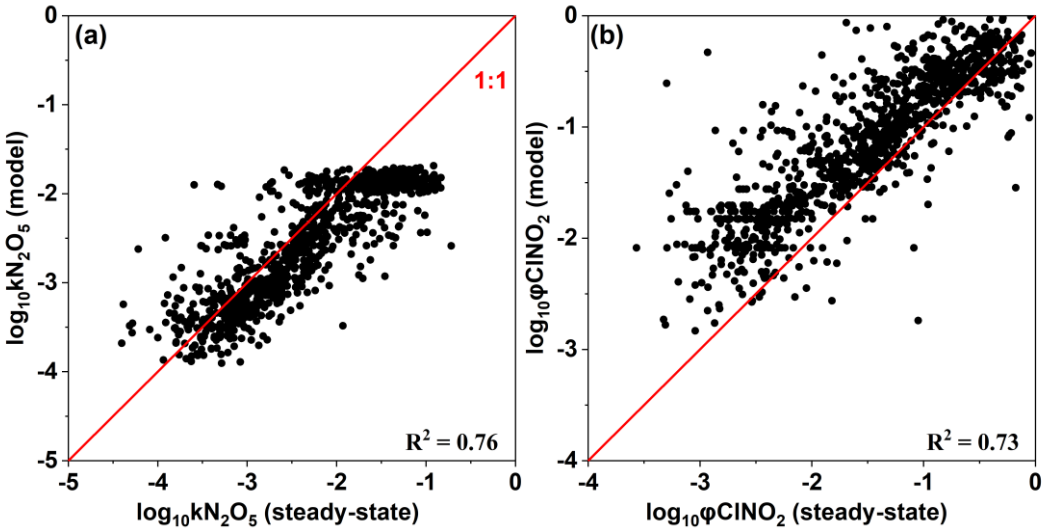

202

203 **Figure S7.** Comparison of parameters derived from iterative box model and steady state approximation

204 method. **(a)** N_2O_5 heterogeneous loss rate and **(b)** $ClNO_2$ production rate, respectively.

205

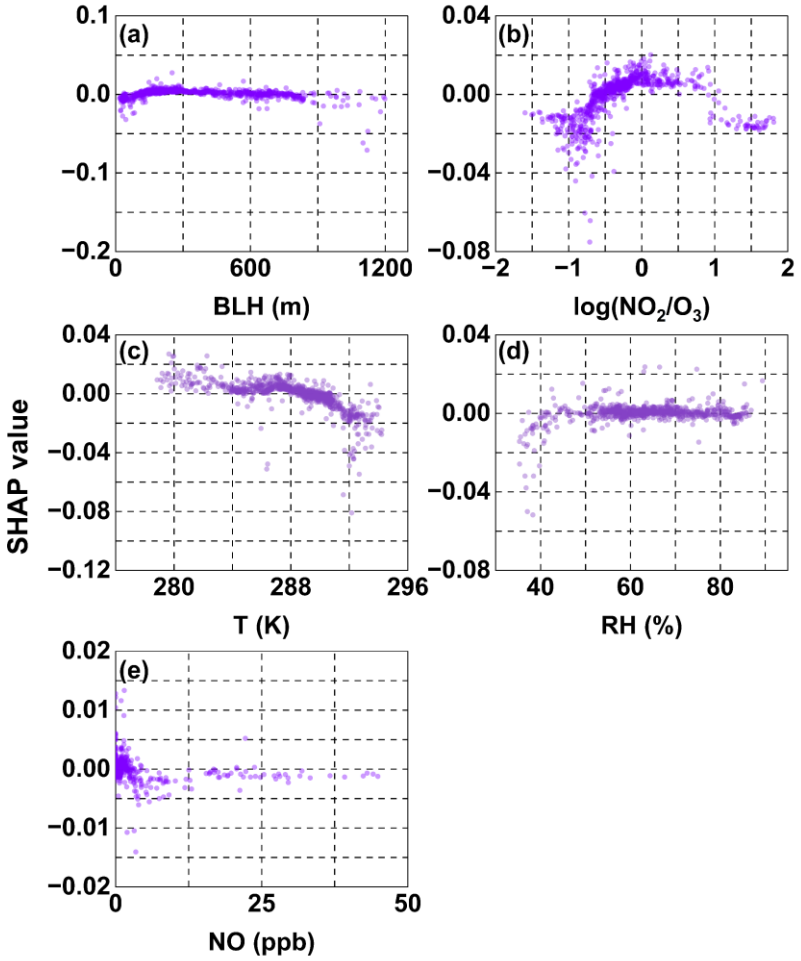

206

207 **Figure S8.** Main effect of the factors **(a)** BLH, **(b)** $\log\frac{NO_2}{O_3}$, **(c)** Temperature, **(d)** RH, and **(e)** NO on the

208 N_2O_5 uptake obtained by XGBoost-SHAP explainer method.

209

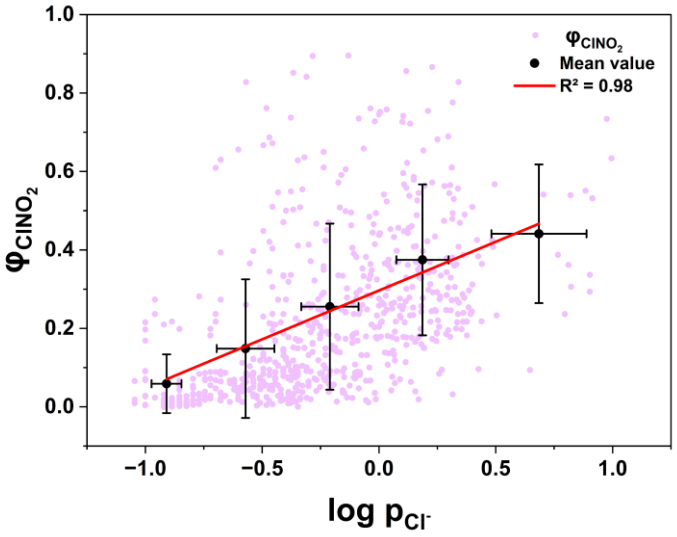

210

Figure S9. The relationship between the log of particulate chlorine ($\log(p_{Cl^-})$) and $\varphi ClNO_2$ in winter 2022. The error bars represent standard deviation, and the black circles are the mean value of each bin, which are (minimum, -0.8], (0.8, -0.4], (-0.4, 0], (0, 0.4], (0.4, maximum] for $\log pCl^-$.

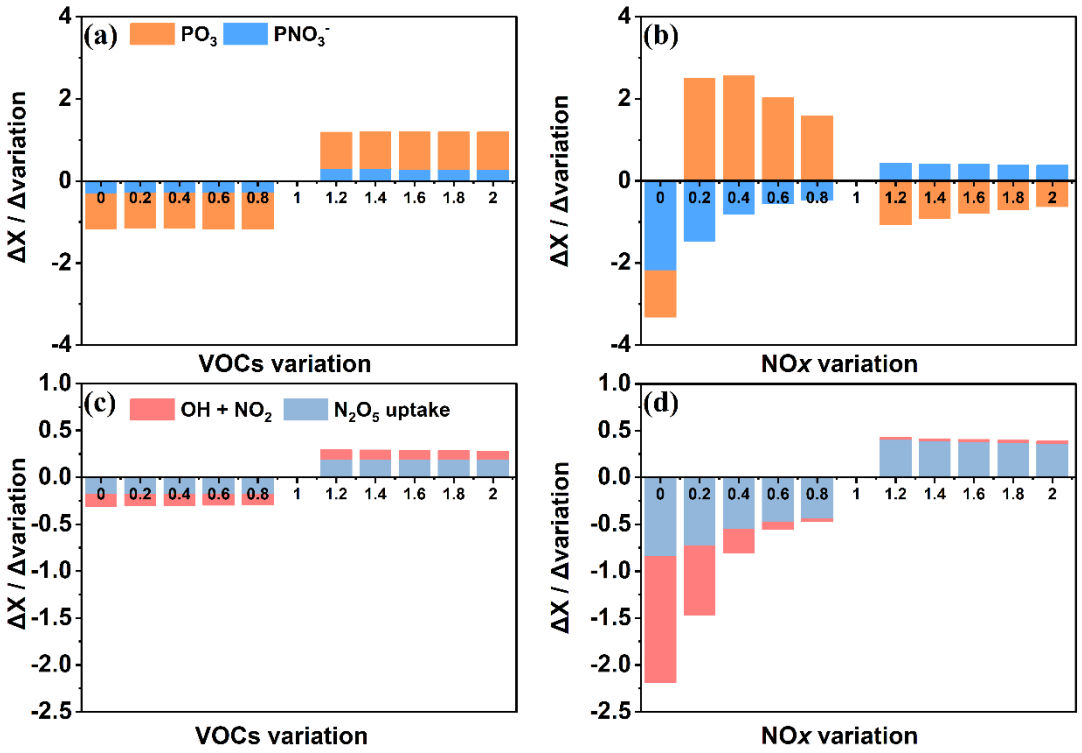

Figure S10. The response strength (RS) of PO_3 and PNO_3^- **(a, b)**, and the RS of the PNO_3^- via N_2O_5 uptake and OH + NO_2 **(c, d)** to different VOCs and NO*x* change scenarios. It's noted that when VOCs change, the emission rate of NO*x* is fixed as base, and when NO*x* change, the emission rate of VOCs is fixed as base.

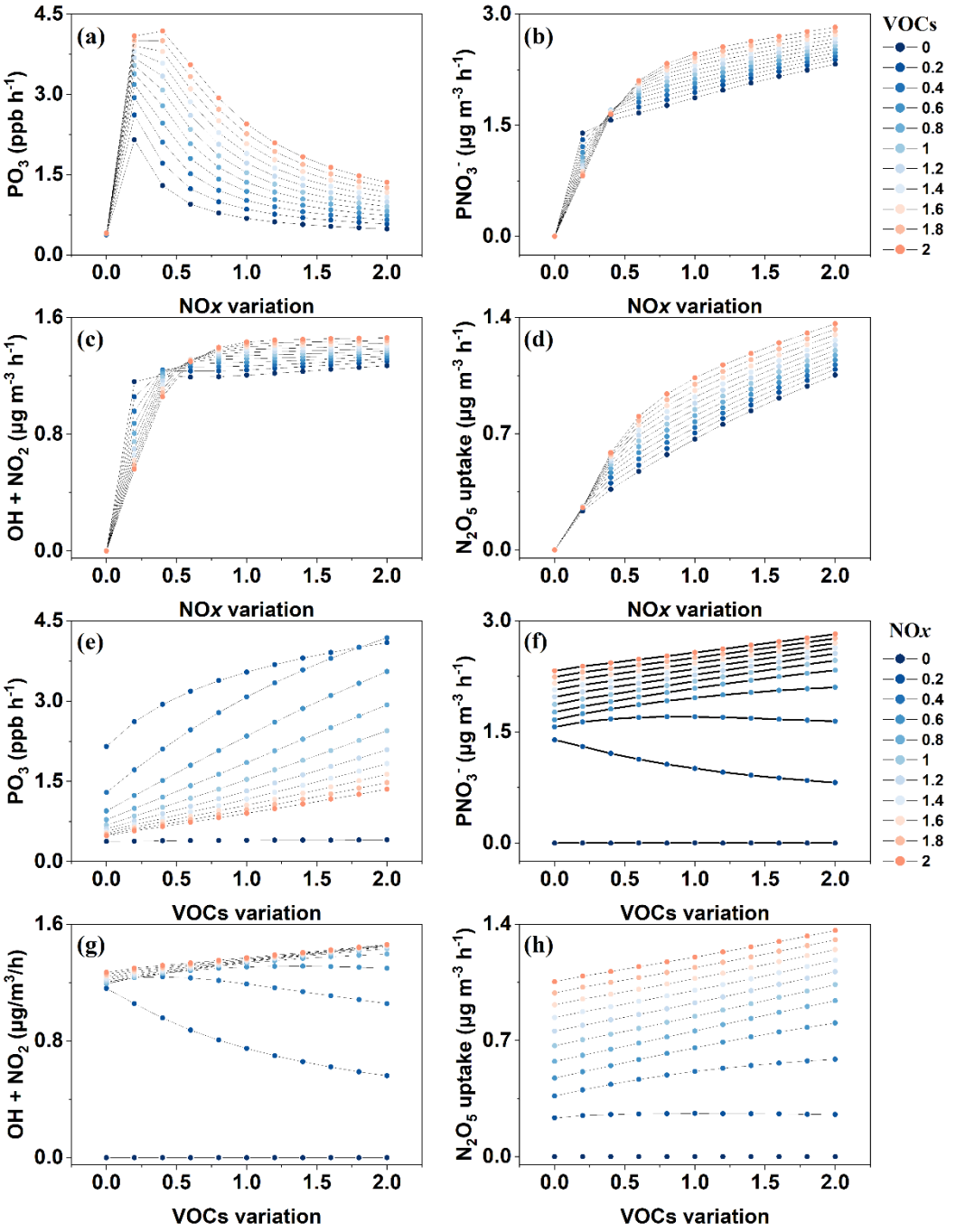

Figure S11. Relationships of mean formation rates of PO_3 **(a, e)**, PNO_3^- **(b, f)**, N_2O_5 uptake **(c, g)**, and OH + NO_2 **(d, h)** to the normalized NO*x* and VOCs in all the examined scenarios simulated by the multiphase chemical box model. The normalized base was the average case of winter 2022.

Table S1. Comparison of the winter NO_2, O_3 and total VOCs levels in urban areas of China.

Location	NO_2 (ppb)	O_3 (ppb)	VOCs (ppb)	$PM_{2.5}$ (μg/m^3)	Observation period	Reference
Xiamen	10.9	27.3	18.2	14.3	Dec,2022 – Feb, 2023	This study

Beijing	-	-	35.8	-	Jan, 2019	(Wei et al., 2021)
Beijing	19.1	9.2	41.2	55.2	Dec, 2018 – Jan, 2019	(Liu et al., 2021b)
Guangzhou	22.9	30.7	33.1	35.5	Jan, 2021	(Cheng et al., 2024)
Nanjing	-	-	40.2	-	Winter, 2016	(Zhao et al., 2020)
Shanghai	22.6	14.1	63.6	34.0	Dec, 2017 – Jan, 2018	(Liu et al., 2021a)
Chengdu	-	-	53.3	-	Jan, 2019	(Xiong et al., 2021)

Table S2. The incorporated mechanism in the F0AM model.

Reaction	Rate constant and emission factor	Reference
$HNO_3 \rightarrow pNO_3^-$	gas-particle partition coefficient	(Zare et al., 2018)
N_2O_5+ aerosol + $H_2O \rightarrow pNO_3^-$	$kN_2O_5 \times (2-\varphi ClNO_2)$	(Chen et al., 2020)
N_2O_5+ aerosol + $pCl^- \rightarrow ClNO_2$	$\varphi ClNO_2$	(Chen et al., 2020)
$ClNO_2$+ hv→ Cl+NO_2	Based on IUPAC	(Sherwen et al., 2016)
Other halogen mechanisms as GEOS-Chem	Based on IUPAC	(Sherwen et al., 2016)

Table S3. Observed period of different winters from 2019 to 2023.

Year	Sampling period
2019	2020.01.01–2020.01.26
2020	2020.12.01–2020.12.14
2021	2022.01.0–2022.02.05
2022	2022.12.01–2023.02.04
2023	2023.12.01–2023.12.31

Supplementary Table 4. Summary of the key parameters of nighttime NO_3-N_2O_5 chemistry around the world. Values of parameters are mean level unless stated.

Region	Site type	Study period	kN_2O_5het (s^{-1})	$\varphi ClNO_2$	Reference
Xiamen, China	Urban	Dec,2022 – Feb,2023	7.64×10^{-3}	0.193	This study
Beijing, China	Rural	May, 2016 – Jun, 2016	8.1×10^{-4}	0.73 ± 0.25	(Wang et al., 2018)
Beijing, China	Urban (vertical)	Oct, 2020 – Nov, 2020	1.42×10^{-3}	-	(Ma et al., 2023)

Hebei, China	Semi-rural	Jun, 2014 – Jul, 2014	1.3×10^{-2}	0.30	(Tham et al., 2016)
Guangdong, China	Semi-rural	Jan, 2017	3.78×10^{-3} – 9.00×10^{-3}	0.18 – 0.32	(Yun et al., 2018)
UK	Flight track	Jul, 2010	9.3×10^{-5} – 0.001	-	(Morgan et al., 2015)

Table S5. Mean concentrations and standard deviations of chemical species and meteorological parameters during the observation period. Concentrations are in ppbv unless stated. The daytime is 07:00 – 17:00 (local time).

Species	Mean	Standard deviation
N_2O_5	0.110	0.215
$ClNO_2$	0.421	0.644
O_3	27.3	14.1
NO	2.83	6.59
NO_2	10.9	6.43
CO	0.409	0.101
SO_2	1.95	0.537
HCHO	1.69	0.858
HONO	0.568	0.519
PAN	0.409	0.302
T (K)	290	4.07
RH (%)	58.3	14
BLH (m)	513	339
P (Pa)	1000	76.6
Calculated $PM_{2.5}$ ($\mu g/cm^3$)	14.3	9.43
C_2H_6	3.04	0.731
C_3H_8	2.74	1.43
NC_4H_{10}	1.19	0.845
IC_4H_{10}	0.808	0.531
NC_5H_{12}	0.302	0.224
IC_5H_{12}	0.673	0.75
C_2H_4	1.14	0.689
C_3H_6	0.313	0.323
C_4H_6	0.0137	0.0174
$CBUT_2ENE$	0.0184	0.0324
$TBUT_2ENE$	0.0139	0.0376
BUT1ENE	0.0641	0.0791
PENT1ENE	0.00471	0.0119
C_5H_8	0.00724	0.0142
CHEX	0.0205	0.0199
NC_6H_{14}	0.107	0.154

M_3PE	0.0751	0.0871
M_2PE	0.0674	0.0827
$M_{23}C_4$	0.0697	0.108
$M_{22}C_4$	0.0261	0.0262
NC_7H_{16}	0.0472	0.0765
M_3HEX	0.0488	0.0888
M_2HEX	0.0334	0.0568
NC_8H_{18}	0.0131	0.0148
NC_9H_{20}	0.00833	0.00986
$NC_{10}H_{22}$	0.00589	0.00652
$NC_{11}H_{24}$	0.00588	0.00742
$NC_{12}H_{26}$	0.02	0.145
HEX1ENE	0.00208	0.00474
C_2H_2	1.09	0.406
BENZENE	0.251	0.107
TOLUENE	0.817	0.992
EBENZ	0.148	0.183
OXYL	0.0888	0.126
PXYL	0.328	0.475
STYRENE	0.0284	0.0663
PBENZ	0.00438	0.00352
IPBENZ	0.00285	0.00374
$TM_{135}B$	0.00529	0.00656
$TM_{124}B$	0.0177	0.0231
$TM_{123}B$	0.005	0.00596
OETHTOL	0.00583	0.00602
METHTOL	0.0105	0.0108
PETHTOL	0.00606	0.0063
ACR	0.0583	0.0417
CH_3COCH_3	1.38	0.743
MEK	0.339	0.321
IPROPOL	0.106	0.152
ETHACET	0.873	1.15
MTBE	0.0939	0.142
CH_3CL	0.0125	0.0132
CH_2CL_2	1.26	1.77
$CHCL_3$	0.038	0.0272
CH_2CLCH_2CL	0.279	0.202
CH_3CH_2CL	0.0156	0.00755
$CL_{12}PROP$	0.101	0.166
TCE	0.0231	0.0246
TRICLETH	0.0111	0.0104
$j_{NO_2}(s^{-1})$ (daytime)	3.76×10^{-3}	3.02×10^{-3}
$j_{O_1D}(s^{-1})$ (daytime)	1.28×10^{-5}	1.25×10^{-5}

j_{HONO}(s^{-1}) (daytime)	6.66×10^{-4}	5.33×10^{-4}
j_{HCHO}(s^{-1}) (daytime)	1.79×10^{-5}	1.47×10^{-5}

Table S6. The average values of key parameters obtained from the interactive box model and the multiphase chemical box model. The daytime in this study is from 7:00 to 17:00.

Parameters	Mean ± standard error
kNO_3(s^{-1})	0.00288 ± 0.00585
kN_2O_5 (s^{-1})	0.00764 ± 0.00612
$\frac{kNO_3}{Keq[NO_2]}$ (s^{-1})	0.000136 ± 0.000306
$\varphi ClNO_2$	0.193 ± 0.284
OH radicals (daytime) (molec m^{-3})	$2.52\times10^6 \pm 2.84\times10^6$
HO_2 radicals (daytime) (molec m^{-3})	$4.24\times10^7 \pm 5.20\times10^7$

References:

Atkinson, R. and Arey, J.: Atmospheric degradation of volatile organic compounds, Chemical Reviews. 103, 4605-4638, https://doi.org/10.1021/cr0206420, 2003.

Brown, S. S., Stark, H., and Ravishankara, A. R.: Applicability of the steady state approximation to the interpretation of atmospheric observations of NO_3 and N_2O_5: art. no. 4539, Journal of Geophysical Research-Atmospheres. 108, https://doi.org/10.1029/2003jd003407, 2003a.

Brown, S. S., Stark, H., Ryerson, T. B., Williams, E. J., Nicks, D. K., Trainer, M., Fehsenfeld, F. C., and Ravishankara, A. R.: Nitrogen oxides in the nocturnal boundary layer:: Simultaneous in situ measurements of NO_3, N_2O_5, NO_2, NO, and O_3 -: art. no. 4299, Journal of Geophysical Research-Atmospheres. 108, https://doi.org/10.1029/2002jd002917, 2003b.

Chen, X. R., Wang, H. C., and Lu, K. D.: Interpretation of NO_3-N_2O_5 observation via steady state in high-aerosol air mass: the impact of equilibrium coefficient in ambient conditions, Atmospheric Chemistry and Physics. 22, 3525-3533, https://doi.org/10.5194/acp-22-3525-2022, 2022.

Chen, X. R., Wang, H. C., Lu, K. D., Li, C. M., Zhai, T. Y., Tan, Z. F., Ma, X. F., Yang, X. P., Liu, Y. H., Chen, S. Y., Dong, H. B., Li, X., Wu, Z. J., Hu, M., Zeng, L. M., and Zhang, Y. H.: Field Determination of Nitrate Formation Pathway in Winter Beijing, Environmental Science & Technology. 54, 9243-9253, https://doi.org/10.1021/acs.est.0c00972, 2020.

Cheng, C. L., Yang, S. X., Yuan, B., Pei, C. L., Zhou, Z. H., Mao, L. Y., Liu, S. L., Chen, D. Y., Cheng, X. Y., Li, M., Shao, M., and Zhou, Z.: The significant contribution of nitrate to a severe haze event in the winter of Guangzhou, China, Science of the Total Environment. 909, https://doi.org/10.1016/j.scitotenv.2023.168582, 2024.

DeMore, W., Howard, C., Sander, S., Ravishankara, A., Golden, D., Kolb, C., Hampson, R., Molina, M., and Kurylo, M.: Chemical Kinetics and Photochemical Data for Use in Stratospheric Modeling, 1997.

Ehhalt, D. H. and Rohrer, F.: Dependence of the OH concentration on solar UV, Journal of Geophysical Research-Atmospheres. 105, 3565-3571, https://doi.org/10.1029/1999jd901070, 2000.

Hu, B. Y., Liu, T. T., Hong, Y. W., Xu, L. L., Li, M. R., Wu, X., Wang, H., Chen, J. H., and Chen, J. S.: Characteristics of peroxyacetyl nitrate (PAN) in a coastal city of southeastern China: Photochemical mechanism and pollution process, Science of the Total Environment. 719,

https://doi.org/10.1016/j.scitotenv.2020.137493, 2020.
Hu, B. Y., Duan, J., Hong, Y. W., Xu, L. L., Li, M. R., Bian, Y. H., Qin, M., Fang, W., Xie, P. H., and Chen, J. S.: Exploration of the atmospheric chemistry of nitrous acid in a coastal city of southeastern China: results from measurements across four seasons, Atmospheric Chemistry and Physics. 22, 371-393, https://doi.org/10.5194/acp-22-371-2022, 2022.
Jenkin, M. E., Young, J. C., and Rickard, A. R.: The MCM v3.3.1 degradation scheme for isoprene, Atmospheric Chemistry and Physics. 15, 11433-11459, https://doi.org/10.5194/acp-15-11433-2015, 2015.
Jenkin, M. E., Saunders, S. M., Wagner, V., and Pilling, M. J.: Protocol for the development of the Master Chemical Mechanism, MCM v3 (Part B): tropospheric degradation of aromatic volatile organic compounds, Atmospheric Chemistry and Physics. 3, 181-193, https://doi.org/10.5194/acp-3-181-2003, 2003.
Liu, T. T., Lin, Y. L., Chen, J. S., Chen, G. J., Yang, C., Xu, L. L., Li, M. R., Fan, X. L., Zhang, F. W., and Hong, Y. W.: Pollution mechanisms and photochemical effects of atmospheric HCHO in a coastal city of southeast China, Science of the Total Environment. 859, https://doi.org/10.1016/j.scitotenv.2022.160210, 2023.
Liu, T. T., Chen, G. J., Chen, J. S., Xu, L. L., Li, M. R., Hong, Y. W., Chen, Y. T., Ji, X. T., Yang, C., Chen, Y. P., Huang, W. G., Huang, Q. J., and Wang, H.: Seasonal characteristics of atmospheric peroxyacetyl nitrate (PAN) in a coastal city of Southeast China: Explanatory factors and photochemical effects, Atmospheric Chemistry and Physics. 22, 4339-4353, https://doi.org/10.5194/acp-22-4339-2022, 2022a.
Liu, T. T., Hong, Y. W., Li, M. R., Xu, L. L., Chen, J. S., Bian, Y. H., Yang, C., Dan, Y. B., Zhang, Y. N., Xue, L. K., Zhao, M., Huang, Z., and Wang, H.: Atmospheric oxidation capacity and ozone pollution mechanism in a coastal city of southeastern China: analysis of a typical photochemical episode by an observation-based model, Atmospheric Chemistry and Physics. 22, 2173-2190, https://doi.org/10.5194/acp-22-2173-2022, 2022b.
Liu, Y. H., Wang, H. L., Jing, S. G., Peng, Y. R., Gao, Y. Q., Yan, R. S., Wang, Q., Lou, S. R., Cheng, T. T., and Huang, C.: Strong regional transport of volatile organic compounds (VOCs) during wintertime in Shanghai megacity of China, Atmospheric Environment. 244, https://doi.org/10.1016/j.atmosenv.2020.117940, 2021a.
Liu, Z. R., Wang, Y. S., Hu, B., Lu, K. D., Tang, G. Q., Ji, D. S., Yang, X. P., Gao, W. K., Xie, Y. Z., Liu, J. Y., Yao, D., Yang, Y., and Zhang, Y. H.: Elucidating the quantitative characterization of atmospheric oxidation capacity in Beijing, China, Science of the Total Environment. 771, https://doi.org/10.1016/j.scitotenv.2021.145306, 2021b.
Ma, P. K., Quan, J. N., Dou, Y. J., Pan, Y. B., Liao, Z. H., Cheng, Z. G., Jia, X. C., Wang, Q. Q., Zhan, J. L., Ma, W., Zheng, F. X., Wang, Y. Z., Zhang, Y. S., Hua, C. J., Yan, C., Kulmala, M., Liu, Y. A., Huang, X., Yuan, B., Brown, S. S., and Liu, Y. C.: Regime-Dependence of Nocturnal Nitrate Formation via N_2O_5 Hydrolysis and Its Implication for Mitigating Nitrate Pollution, Geophysical Research Letters. 50, https://doi.org/10.1029/2023gl106183, 2023.
Morgan, W. T., Ouyang, B., Allan, J. D., Aruffo, E., Di Carlo, P., Kennedy, O. J., Lowe, D., Flynn, M. J., Rosenberg, P. D., Williams, P. I., Jones, R., McFiggans, G. B., and Coe, H.: Influence of aerosol chemical composition on N_2O_5 uptake: airborne regional measurements in northwestern Europe, Atmospheric Chemistry and Physics. 15, 973-990, https://doi.org/10.5194/acp-15-973-2015, 2015.
Niu, Y. B., Zhu, B., He, L. Y., Wang, Z., Lin, X. Y., Tang, M. X., and Huang, X. F.: Fast Nocturnal

Heterogeneous Chemistry in a Coastal Background Atmosphere and Its Implications for Daytime Photochemistry, Journal of Geophysical Research-Atmospheres. 127, https://doi.org/10.1029/2022jd036716, 2022.
Shapley, L. S.: A value for n-person games, Contributions to the Theory of Games. 1953.
Sherwen, T., Schmidt, J. A., Evans, M. J., Carpenter, L. J., Grossmann, K., Eastham, S. D., Jacob, D. J., Dix, B., Koenig, T. K., Sinreich, R., Ortega, I., Volkamer, R., Saiz-Lopez, A., Prados-Roman, C., Mahajan, A. S., and Ordóñez, C.: Global impacts of tropospheric halogens (Cl, Br, I) on oxidants and composition in GEOS-Chem, Atmospheric Chemistry and Physics. 16, 12239-12271, https://doi.org/10.5194/acp-16-12239-2016, 2016.
Thaler, R. D., Mielke, L. H., and Osthoff, H. D.: Quantification of Nitryl Chloride at Part Per Trillion Mixing Ratios by Thermal Dissociation Cavity Ring-Down Spectroscopy, Analytical Chemistry. 83, 2761-2766, https://doi.org/10.1021/ac200055z, 2011.
Tham, Y. J., Wang, Z., Li, Q. Y., Yun, H., Wang, W. H., Wang, X. F., Xue, L. K., Lu, K. D., Ma, N., Bohn, B., Li, X., Kecorius, S., Grösss, J., Shao, M., Wiedensohler, A., Zhang, Y. H., and Wang, T.: Significant concentrations of nitryl chloride sustained in the morning: investigations of the causes and impacts on ozone production in a polluted region of northern China, Atmospheric Chemistry and Physics. 16, 14959-14977, https://doi.org/10.5194/acp-16-14959-2016, 2016.
Wang, H. C., Peng, C., Wang, X., Lou, S. R., Lu, K. D., Gan, G. C., Jia, X. H., Chen, X. R., Chen, J., Wang, H. L., Fan, S. J., Wang, X. M., and Tang, M. J.: N_2O_5 uptake onto saline mineral dust: a potential missing source of tropospheric $ClNO_2$ in inland China, Atmospheric Chemistry and Physics. 22, 1845-1859, https://doi.org/10.5194/acp-22-1845-2022, 2022a.
Wang, H. C., Lu, K. D., Guo, S., Wu, Z. J., Shang, D. J., Tan, Z. F., Wang, Y. J., Le Breton, M., Lou, S. R., Tang, M. J., Wu, Y. S., Zhu, W. F., Zheng, J., Zeng, L. M., Hallquist, M., Hu, M., and Zhang, Y. H.: Efficient N_2O_5 uptake and NO_3 oxidation in the outflow of urban Beijing, Atmospheric Chemistry and Physics. 18, 9705-9721, https://doi.org/10.5194/acp-18-9705-2018, 2018.
Wang, H. C., Yuan, B., Zheng, E., Zhang, X. X., Wang, J., Lu, K. D., Ye, C. S., Yang, L., Huang, S., Hu, W. W., Yang, S. X., Peng, Y. W., Qi, J. P., Wang, S. H., He, X. J., Chen, Y. B., Li, T. G., Wang, W. J., Huangfu, Y. B., Li, X. B., Cai, M. F., Wang, X. M., and Shao, M.: Formation and impacts of nitryl chloride in Pearl River Delta, Atmospheric Chemistry and Physics. 22, 14837-14858, https://doi.org/10.5194/acp-22-14837-2022, 2022b.
Wang, Z., Wang, W. H., Tham, Y. J., Li, Q. Y., Wang, H., Wen, L., Wang, X. F., and Wang, T.: Fast heterogeneous N_2O_5 uptake and $ClNO_2$ production in power plant and industrial plumes observed in the nocturnal residual layer over the North China Plain, Atmospheric Chemistry and Physics. 17, 12361-12378, https://doi.org/10.5194/acp-17-12361-2017, 2017.
Wei, W., Wang, Y., Bai, H. X., Wang, X. Q., Cheng, S. Y., and Wang, L. T.: Insights into atmospheric oxidation capacity and its impact on $PM_{2.5}$ in megacity Beijing via volatile organic compounds measurements, Atmospheric Research. 258, https://doi.org/10.1016/j.atmosres.2021.105632, 2021.
Xiong, C., Wang, N., Zhou, L., Yang, F. M., Qiu, Y., Chen, J. H., Han, L., and Li, J. J.: Component characteristics and source apportionment of volatile organic compounds during summer and winter in downtown Chengdu, southwest China, Atmospheric Environment. 258, https://doi.org/10.1016/j.atmosenv.2021.118485, 2021.
Yang, C., Dong, H. S., Chen, Y. P., Xu, L. L., Chen, G. J., Fan, X. L., Wang, Y. H., Tham, Y. J., Lin, Z. Y., Li, M. R., Hong, Y. W., and Chen, J. S.: New Insights on the Formation of Nucleation Mode Particles in a Coastal City Based on a Machine Learning Approach, Environmental Science & Technology. 58,

1187-1198, https://doi.org/10.1021/acs.est.3c07042, 2023.
Yun, H., Wang, W. H., Wang, T., Xia, M., Yu, C., Wang, Z., Poon, S. C. N., Yue, D. L., and Zhou, Y.: Nitrate formation from heterogeneous uptake of dinitrogen pentoxide during a severe winter haze in southern China, Atmospheric Chemistry and Physics. 18, 17515-17527, https://doi.org/10.5194/acp-18-17515-2018, 2018.
Zare, A., Romer, P. S., Nguyen, T., Keutsch, F. N., Skog, K., and Cohen, R. C.: A comprehensive organic nitrate chemistry: insights into the lifetime of atmospheric organic nitrates, Atmospheric Chemistry and Physics. 18, 15419-15436, https://doi.org/10.5194/acp-18-15419-2018, 2018.
Zhao, Q. Y., Bi, J., Liu, Q., Ling, Z. H., Shen, G. F., Chen, F., Qiao, Y. Z., Li, C. Y., and Ma, Z. W.: Sources of volatile organic compounds and policy implications for regional ozone pollution control in an urban location of Nanjing, East China, Atmospheric Chemistry and Physics. 20, 3905-3919, https://doi.org/10.5194/acp-20-3905-2020, 2020.